INCLUSION PHENOMENA AND MOLECULAR RECOGNITION

Edited by

Jerry L. Atwood
University of Alabama
Tuscaloosa, Alabama

PLENUM PRESS • NEW YORK AND LONDON

CONTENTS

New Shapes for Catalysis and Molecular Recognition 1
J. Rebek, Jr.

"Artificial Oligonucleotides": Molecular Recognition by Base Pairing 17
J. L. Sessler and D. Magda

Optimizing the Neutral Molecular Receptor Properties of Water Soluble Cyclophanes 27
Craig S. Wilcox, Marlon D. Cowart, Irving Sucholeiki, Rudolf R. Bukownik, and Vincent Lynch

Complexation and Molecular Recognition of Neutral and Anionic Substrates in the Solid and Solution States by Bisparaquat(1,4)cyclophane 41
Mark V. Reddington, Neil Spencer, and J. Fraser Stoddart

The Hexagonal Lattice Approach to Molecular Receptors 49
Thomas W. Bell, Albert Firestone, Jia Liu, Richard Ludwig, and Scott D. Rothenberger

Molecular Recognition by Macrocyclic Receptors 57
Andrew D. Hamilton

Host-Guest Binding Mechanisms: Experimental Approaches 65
Hans-Jörg Schneider, Thomas Blatter, Rüdiger Kramer, Surat Kumar, Ulrich Schneider, and Isolde Theis

Designed DNA Interactions 75
Kent D. Stewart

A Novel Application of the Host-Guest Paradigm: Design of Organic Optoelectronic Materials 81
David M. Walba, Noel A. Clark, Homaune A. Razavi, and Devendra S. Parmar

Complexes of Neutral Molecules and Cyclophane Hosts 93
François Diederich

Catalytic Functions of Paracyclophanes Based on Molecular Recognition 107
Yukito Murakami

Synthesis and Complexing Properties of Chiral Guanidinium Receptors Designed for Molecular Recognition of Anions 119
Antonio Echavarren, Amalia Galán, Jean-Marie Lehn, and Javier de Mendoza

Molecular Design of Calixarene-Based Host Molecules 125
Seiji Shinkai

Complexation of Ions and Neutral Molecules by Functionalized Calixarenes 135
Rocco Ungaro, Andrea Pochini, and Arturo Arduini

Biomimetic Ion Transport: Pores and Channels in Vesicle Membranes 145
V. E. Carmichael, P. J. Dutton, T. M. Fyles, T. D. James,
C. McKim, J. A. Swan, and M. Zojaji

Thermodynamics of Micellization for the K^+ and Ba^{2+} Complexes of a Lipophilic Cryptand 151
Lourdes E. Echegoyen, Steve R. Miller, George W. Gokel, and Luis Echegoyen

Redox Active Crowns: Towards the Second Generation 161
Stephen R. Cooper

Heavy Metal Chemistry of Mixed Donor Macrocyclic Ligands: Strategies for Obtaining Metal Ion Recognition 171
Leonard F. Lindoy

Lanthanide Chelates as Luminescent Probes 185
John L. Toner

Catalytic Reactions of Macrocyclic Nickel(II) Complexes 199
Cynthia J. Burrows

Shape Selective Oxidation as a Mechanistic Probe 209
Kenneth S. Suslick and Bruce R. Cook

Novel Chromogenic Ionophores for Determination of Sodium and Potassium in Biological Fluids: Synthesis and Applications 217
Donald J. Cram, Eddy Chapoteau, Bronislaw P. Czech, Carl R. Gebauer, Roger C. Helgeson, and Anand Kumar

From Real Chymotrypsin to Artificial Chymotrypsin: Myron L. Bender's Legacy 227
Valerian T. D'Souza

Molecular Recognition by Cyclodextrin Hosts: Approach to New Functions 237
Iwao Tabushi, Kazuo Yamamura, and Yasuhisa Kuroda

Fluorescence and Circular Dichroism Studies on Molecular and Chiral Recognition by Cyclodextrins 243
Koji Kano

The Interactions of Vesicle-Forming Surfactants with Cyclodextrins 251
Orlando Garcia, Pablo A. Quintela, Jodi M. Schuette, Rafael Vargas, Hae R. Yoon, and Angel E. Kaifer

Biomedical Uses of Amorphous Water-Soluble Derivatives of Cyclodextrins 261
Josef Pitha

Inclusion and Reaction Chemistry of Two Anthracene-Appended γ-Cyclodextrins 269
Akihiko Ueno, Fumio Moriwaki, Akiko Azuma, and Tetsuo Osa

Computer Simulations of Host-Guest Complexes 277
A. K. Cheetham and B. K. Peterson

Photochemistry of Organic Molecules Adsorbed on Faujasite Zeolites: Steric Effects on Product Distributions 289
Nicholas J. Turro

High Resolution Solid State NMR Studies of the Effect of Temperature and Adsorbed Organic Molecules on Zeolite Lattice Structures 299
C. A. Fyfe, G. T. Kokotailo, H. Gies, and H. Strobl

Motion of Organic Species Occluded or Sorbed within Zeolites 325
J. M. Newsam, B. G. Silbernagel, M. T. Melchior, T. O. Brun, and F. Trouw

Inclusion of Organometallics in Zeolite Host Structures 339
Thomas Bein, Karin Moller, and Aticha Borvornwattananont

Photochemistry in Zeolite Cavities 351
V. Ramamurthy

Artificial Photosynthesis in Zeolite-Based Molecular Assemblies 365
Jonathan S. Krueger, Cuiwei Lai, Zhuyin Li, James E. Mayer, and Thomas E. Mallouk

Silver Sodalites: Novel Optically Responsive Nanocomposites 379
Geoffrey A. Ozin, Andreas Stein, Galen D. Stucky, and John P. Godber

Surface Enhanced Luminescence with Silver Exchanged Zeolites 395
James F. Tanguay and Steve L. Suib

Size Quantized Semiconductors in Porous Hosts - Quantum Dots 401
Norman Herron and Ying Wang

Index 409

INCLUSION OF ORGANOMETALLICS IN ZEOLITE HOST STRUCTURES

Thomas Bein,* Karin Moller, and Aticha Borvornwattananont

Department of Chemistry
University of New Mexico
Albuquerque, New Mexico 87131 (USA)

SUMMARY

An overview is given on new synthetic strategies to stabilize organometallic fragments in the cage system of large-pore zeolites. A common theme is the utilization of intrazeolite bridged hydroxyl groups as reactive centers for surface chemistry. The intracavity chemistry of $[CpFe(CO)_2]_2$ (Fp2), $COTFe(CO)_3$ (COT), $CpFe(CO)_2CH_3$ and ferrocene in different acid forms of zeolite Y has been studied with EXAFS, in situ FTIR, and TPD-MS spectroscopies. Depending on the stoichiometry of zeolite protons vs. the amount of starting complex, different reaction routes are observed, including oxidative cleavage or protonation of Fp2 and ligand rearrangement of COT. The stability of all complexes is influenced by the intracavity concentration of the zeolite bridged hydroxyl groups. Upon treatment at higher temperatures under vacuum, carbonyl and other ligands split off from the complexes and the remaining fragments attach to the zeolite host structure via oxygen coordination. These fragments are stabilized against migration and agglomeration.

INTRODUCTION

Much recent work has been devoted to the immobilization of organometallic catalysts on solid supports. The incentive for these research efforts is based upon the notion that it should be possible to combine the advantages of homogeneous catalysts, such as high selectivity, mild reaction conditions, or the potential utilization of all metal atoms, with those of heterogeneous systems, i.e., facile product separation, facile recovery of the expensive catalyst, and inherent stability. The new 'hybrid' systems derived from this strategy could even offer potential new, desirable features such as stabilization against aggregation, or greater flexibility in the choice of reaction media. However, hybrid systems can also present complications, including the almost ubiquitous instability against leaching of the catalyst metal into solution, agglomeration resulting in (undesired) metal particles, and failure to achieve true site isolation (on organic supports).

Inclusion Phenomena and Molecular Recognition
Edited by J. Atwood
Plenum Press, New York, 1990

In contrast to their amorphous counterparts, zeolite molecular sieves are highly crystalline oxides with well-defined pore sizes of typical molecular dimensions. They offer an enormous variety in pore structures and dimensions, allow controlled modifications of the internal surface, and in many cases show substantial thermal and chemical stability. In addition to the potential advantages of conventional hybrid systems, intrazeolite catalysts offer diffusional shape selectivity for substrate and product molecules, selectivity of polar vs. nonpolar substrates, and in favorable cases so-called 'transition state selectivity' which affects the transition state of the catalytic reaction. The following intrazeolite deposition concepts for catalytically active centers can be distinguished:

1. *Physisorption.* Neutral metal carbonyls have been adsorbed in large-pore zeolites, primarily in faujasite-type structures [1,2]. We have recently shown that zeolite metal cations such as Na^+ provide weak binding sites for the carbonyl ligands [3]. However, this interaction does not prevent carbonyl complexes such as $Ni(CO)_4$ [4], $Fe(CO)_5$, or $Mo(CO)_6$ from diffusion, migration out of the pore system, and eventual agglomeration at elevated temperatures [5,6].

2. A stronger, electrostatic binding mode to the anionic framework is achieved with *cationic transition metal species.* Here, transition metal cations are introduced into the zeolite framework via aqueous ion exchange and subsequently exposed to CO to form carbonyl complexes. Intrazeolite Ru [7], Ir [8], and particularly Rh carbonyl complex cations have been studied in great detail [9-11]. Migration of intrazeolite Rh-carbonyl species and eventual formation of extrazeolite Rh(0) particles appears to occur under the experimental conditions used for catalytic hydroformylation reactions [12]. The structural instability of the Rh-CO-zeolite system presents major limitations towards utilization of the intrazeolite pore structure for shape-selective catalytic reactions. The ion exchange and dehydration steps applied in metal-ion precursor concepts do not offer much control over the siting of the metal species because the metal ions typically migrate into stable positions in smaller cages upon dehydration.

3. Recently, the immobilization of intrazeolite complexes by *diffusional blocking* ("ship in the bottle") has been explored. This approach requires a rigid ligand sphere as present in phthalocyanine (Pc) and other chelate complexes. Intrazeolite Co(II)salen prepared by Co(II) ion exchange and successive reaction with the ligand was found to bind molecular oxygen [13], and intrazeolite Co- [14] and Fe-Pc [15] complexes showed catalytic activity in selective olefin oxidations. Critical issues include potential pore-blocking by the large complex (only three-dimensional or two-dimensional networks can be used with very low concentrations of the complex), and limited substrate access to the catalytically active metal center. In some cases, the severe synthesis conditions can cause local lattice breakdown and inhomogeneous siting.

4. Anchoring concepts based upon *bridged zeolite hydroxyl groups.* In view of the preceding discussion it becomes clear that a qualitative improvement is needed to form stable

inclusions of organometallics in the zeolite pore system. We explore an anchoring concept which utilizes the bridged hydroxyl groups present in the acid forms of many zeolite structure types. The protons located at the zeolite Si-O-Al bridges are highly acidic. The acid sites represent an attractive, largely unexplored type of reactive site for attaching organometallic fragments, with the following potential advantages: Since small species can be anchored, pore clogging can be avoided and a homogeneous site distribution is likely. A variety of metals, ligands, and attachment chemistry can be explored, and the mild reaction conditions allow to direct the metal siting into the large cage systems.

In analogy to the surface chemistry of transition metal allyl complexes on amorphous oxide supports [16-18] the reaction of $Rh(allyl)_3$ with partially proton-exchanged X and Y type zeolite has been reported [19-22]. The formation of intrazeolite Rh-CO and -hydride species as inferred from infrared data indicated that the anchored Rh-allyl fragment reacted similarly to the complex in solution. Preferential hydrogenation of *n*-olefins vs. large cycloolefins suggested that the catalytically active sites were indeed located and accessible in the zeolite pore structure. Structural information about these systems is still lacking.

We study the different relative reactivities and stabilities of ligands at a metal center with respect to the bridged intrazeolite hydroxyls as a basis for the rational design of zeolite based hybrid catalysts. Reactions of $[CpFe(CO)_2]_2$ [23], $COTFe(CO)_3$ [24], $CpFe(CO)_2CH_3$ and ferrocene in different acid forms of zeolite Y are described in the following.

EXPERIMENTAL

Sample preparation: Four different supports based upon Y zeolite were used in this study: NaY (commercial Linde LZ-Y52, $[Na_{57}Al_{57}Si_{135}O_{384}]$ x 235 H_2O), partially proton exchanged H2Y derived from LZ-Y52 via ion exchange with 2 NH_4^+ per supercage, and highly acidic H6Y (6 H^+/sc, sc = supercage) derived from Linde LZ-Y62, $[(NH_4)_{45}Na_{10}Al_{55}Si_{137}O_{384}]$ x 235 H_2O. Heating under vacuum at 1K/min up to 700 K gave the desired acid form of the zeolite. EXAFS samples were derived from proton-exchanged, thermally stabilized zeolite Linde LZ-Y72 with a Si/Al ratio of 2.55 (HY). With $[CpFe(CO)_2]_2$ and $FeCp_2$, the EXAFS samples showed IR spectra corresponding to those obtained with H2Y. With $COTFe(CO)_3$ they were equivalent to those obtained with H6Y. Loading with the complexes was accomplished by stirring a slurry of 0.500 g of zeolite with the required amounts of organometallic compound in 50 mL of hexane for twelve hours under nitrogen. The three supports were loaded at an average level of 0.5 molecules of $[CpFe(CO)_2]_2$ (Fp2), 1 molecule of $COTFe(CO)_3$ (COT), and 1 molecule of $CpFe(CO)_2CH_3$ (MeFp) per supercage. Ferrocene ($FeCp_2$) concentrations were formally 2 molecules per supercage.

FTIR-TPD-MS: FTIR data were obtained with a Mattson Polaris spectrometer at 4 cm^{-1} resolution. Thin dispersions of the zeolite samples on Si wafers were heated at 1 K/min in an in-situ cell connected to an ultrahigh vacuum thermodesorption apparatus combined with a quadrupole mass spectrometer (Dycor M200, 1-200 amu).

EXAFS: EXAFS measurements of sealed samples were performed at NSLS Brookhaven National Laboratories at beamline X-11A with a stored electron energy of 2.5 GeV and ring currents between 60-110 mA. Fe K-edge data at 7112 eV were collected at about 100 K in transmission using a Si(400) monochromator. The EXAFS data were analyzed following standard procedures [25].

RESULTS AND DISCUSSION

Intrazeolite Reactions of $[CpFe(CO)_2]_2$ at Room Temperature

The adduct between Fp2 and NaY is characterized by a shift of the CO stretching frequencies with respect to the unsupported complex (Figure 1a). This indicates an interaction between the Na^+ ions and the CO ligands (see discussion for COT). The oxidative cleavage reactions of $[CpFe(CO)_2]_2$ in homogeneous medium have been reported [26-30]. The dimer reacts in $HCl/CHCl_3$ to $CpFe(CO)_2Cl$, which forms the tricarbonyl cation $CpFe(CO)_3^+$ under CO pressure [31]. Proton exchanged zeolites ($pK_a < -3$) represent solid acids of strength comparable to concentrated mineral acids [32]. It is found in this study that the tricarbonyl cation forms in the pores of the acid zeolite hosts H2Y and H6Y via oxidation of the precursor dimer at room temperature (IR spectra are shown in Figure 2). The EXAFS data of sample H2Y/Fp2 agree very well with this reaction path as described in the following: the

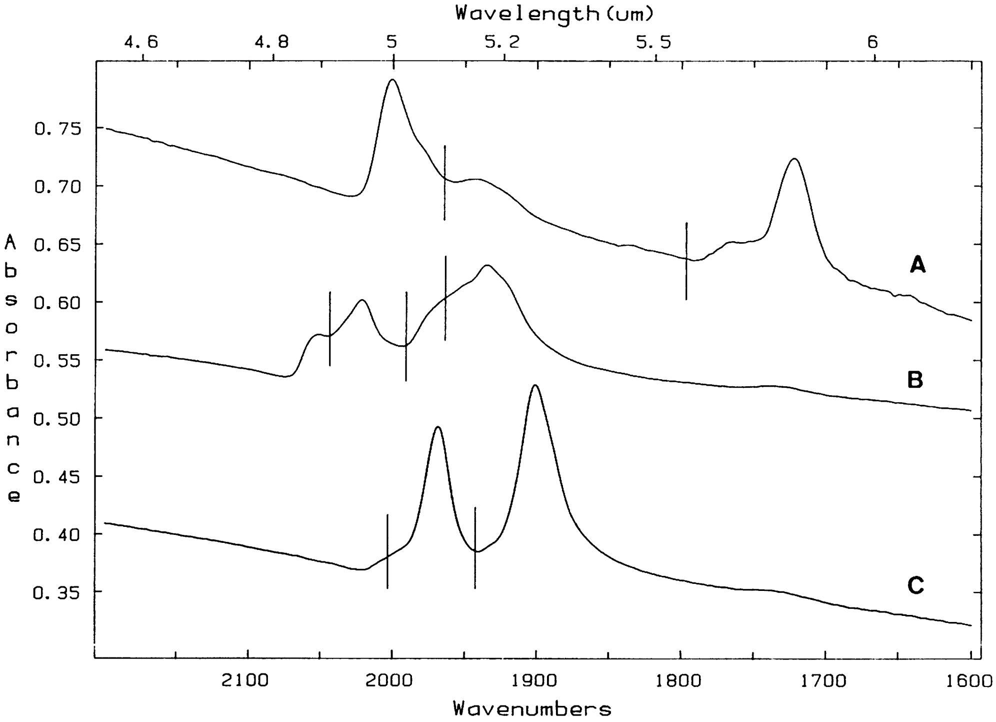

Figure 1. FTIR spectra of a) $[CpFe(CO)_2]_2$, b) $COTFe(CO)_3$ and c) $CpFe(CO)_2CH_3$ in the neutral zeolite matrix NaY at room temperature. Markers indicate the literature values of the unsupported complexes in KBr.

intensity of the iron-iron scatterer pair observed in the EXAFS spectrum of the unsupported complex is reduced to 20% after adsorption into the zeolite, indicating cleavage of the metal-metal bonds of the dimer. Coordination distances and numbers are in line with the formation of $CpFe(CO)_3^+$. The EXAFS data are consistent with the presence of about 40% $CpFe(CO)_3^+$, 40% $CpFe(OZ)_2$, and a remainder of 20% of the dimer (OZ: zeolite oxygen atoms). The formation of the cationic complex $CpFe(CO)_3^+$ is not only determined by the relative concentration and strength of intrazeolite acid groups present, but it is also kinetically controlled (adsorbed water does not affect this process).

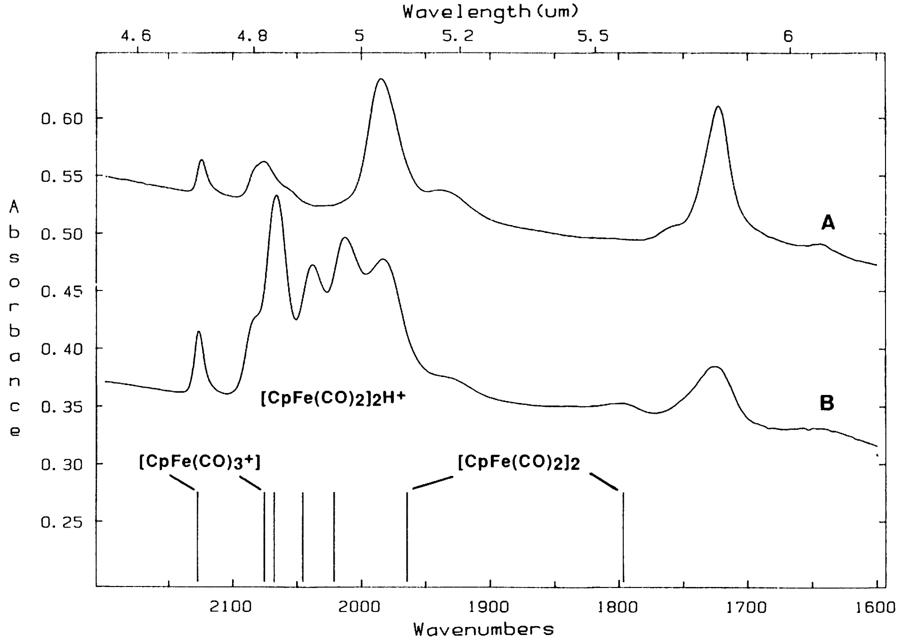

Figure 2. FTIR spectra of $[CpFe(CO)_2]_2$ in acid supports at room temperature. A) in H2Y and b) in H6Y. Markers indicate the literature values for $CpFe(CO)_3^+$ (H_2SO_4 film), $[Cp(CO)_2Fe]_2H^+$ (CH_2Cl_2), and $[CpFe(CO)_2]_2$ (KBr).

Based upon the combined EXAFS and FTIR/TPD-MS data it is demonstrated that the reactivity of the original complex $[CpFe(CO)_2]_2$ is very dependent upon the concentration of acid hydroxyls offered by the solid reaction medium. An increasing relative amount of protons favors the oxidation of the dimer to the monomeric cation. The zeolite host H6Y with even higher proton activity opens a reaction path to form the protonated dimer $[Cp(CO)_2Fe]_2H^+$ (Figure 2b). The analogous reaction in homogeneous medium has been described in a recent publication [33]. The intrazeolite reactions of $[CpFe(CO)_2]_2$ at room temperature can be understood according to the tentative reaction pathways shown in Equations (1) and (2):

medium acidity (H2Y/Fp2):

$[CpFe(CO)_2]_2 + 2\ ZOH + OZ \rightarrow [CpFe(CO)_3]^+OZ^- + H_2 + CO + CpFe(OZ)_2$ (1)
(ZOH, zeolite bridged hydroxyls)

high excess of protons (H6Y/Fp2):

$[CpFe(CO)_2]_2 + x\ ZOH \rightarrow \{[Cp(CO)_2Fe]_2H\}^+OZ^- + (x-1)\ ZOH$ (2)

Intrazeolite Reactions of $[CpFe(CO)_2]_2$ at Elevated Temperatures

If sample H2Y/Fp2 is heated at 473 K for 10 hours, striking changes of the EXAFS data can be observed (compare Figure 3a,b). The small Fe-Fe backscattering contribution and that from linear CO ligands present at room temperature are eliminated. Two peaks near the

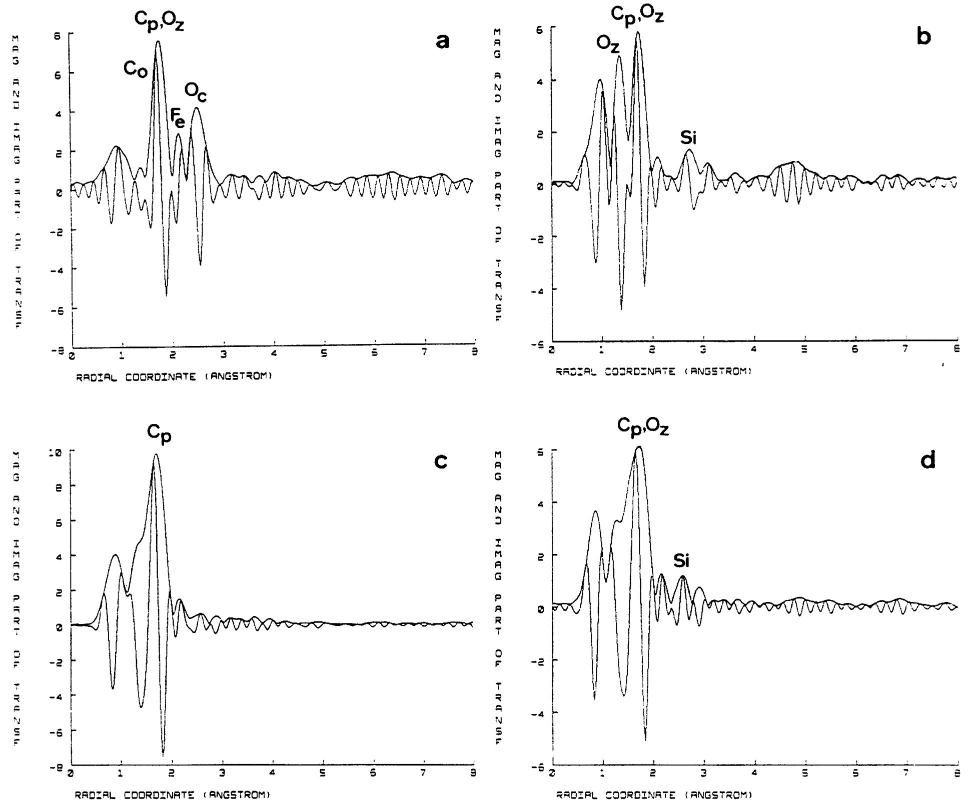

Figure 3. Iron EXAFS spectra of a,b) $[CpFe(CO)_2]_2$ at room temperature and 473 K, and c,d) ferrocene at room temperature and 573 K, in acid support HY. The magnitudes and imaginary parts of the k^3 weighted Fourier transformations are shown. The spectra are uncorrected for phase shifts. Labels indicate the following backscatterers: Co = Fe-CO, Cp = Fe-Cp, Fe = Fe-Fe, Oz = Fe-O(zeolite), Oc = Fe-CO, Si = Fe-Si/Al. Some peaks are convoluted and labels indicate the positions obtained from the EXAFS analysis.

position of the original Fe-Cp shell are now dominant (Figure 3b). The fitting routine deconvolutes these peaks, indicating as the major contribution an Fe-Cp fragment at 2.07 Å. An optimum fit was derived with two additional Fe-O contributions, indicating the presence of two species, i.e. bare iron ions at 1.93 Å plus $CpFe(OZ)_n$ at 2.16 Å. A smaller peak at about 2.8 Å is clearly visible at this temperature and is assigned to backscattering from the zeolite framework metals Si or Al. The combined appearance of these new peaks is a strong indication for coordination of the resulting complex fragments to zeolite cation sites [34]. As confirmed by FTIR measurements, the tricarbonyl cation thus splits off all CO ligands at higher temperatures. However, no Cp fragments are detected in the vapor phase, and the EXAFS analysis indicates that the Cp ligands are still coordinated to the iron metal to form the "half-sandwich" $CpFe^+(OZ)n^-$, anchored to the oxygen rings present in the zeolite supercage. The EXAFS data suggest that n is between two and three, depending on the fraction of bare iron ions. The limited accuracy of EXAFS coordination numbers and the potential presence of several sites does not allow precise determination of the partition of the CpFe fragments between 4-ring (SIII) and 6-ring (SII) sites. Ferrocene was found to give the same fragment at 473 K. Only two zeolite oxygens were coordinated to the Fe in this case, indicating attachment to the SIII sites (Figure 3 c,d). The combined presence of Fe^{2+} and $CpFe(OZ)_2$ fragments and the results discussed above are consistent with the following decomposition reactions of Fp2:

$$[CpFe(CO)_2]_2 + 4\,HOZ \xrightarrow{470\ K} 4\,CO(g) + 2\,CpH + 2\,Fe^{2+}(OZ)_2 + H_2$$

$$[CpFe(CO)_3]^+OZ^- + OZ \xrightarrow{470\ K} 3\,CO(g) + CpFe(OZ)_2$$

Intrazeolite Chemistry of $COTFe(CO)_3$

As observed with $[CpFe(CO)_2]_2$, the chemistry of $COTFe(CO)_3$ in the large pore zeolite Y environment is determined by the concentration of framework protons present. In NaY, the complex is believed to reside in two forms. A majority of the complex molecules is shielded from interactions with the sodium cations by other molecules and thus exhibits only slightly perturbed CO vibrations (Figure 1b). A closer contact to the zeolite "walls", however, leads to a stronger interaction between the CO ligands and the Na^+ cations such as Na···OC-Fe which resembles contact ion-pair interactions of carbonyl complexes with alkali cations in solution [35] and results in a lower symmetry of the complex, split peaks and lower frequencies. Similar effects of lowered symmetry and band splitting were found in an earlier study of nickel carbonyl complexes in different zeolite supports [3]. As indicated by the IR and EXAFS data, in sample H6Y/COT the absence of sodium ions and the high level of protons result in the exclusive formation of bicyclo [5.1.0] octadienyl iron tricarbonyl cation $[C_8H_9Fe(CO)_3]^+$ (homotropylium iron tricarbonyl; Figure 4a, 5b).

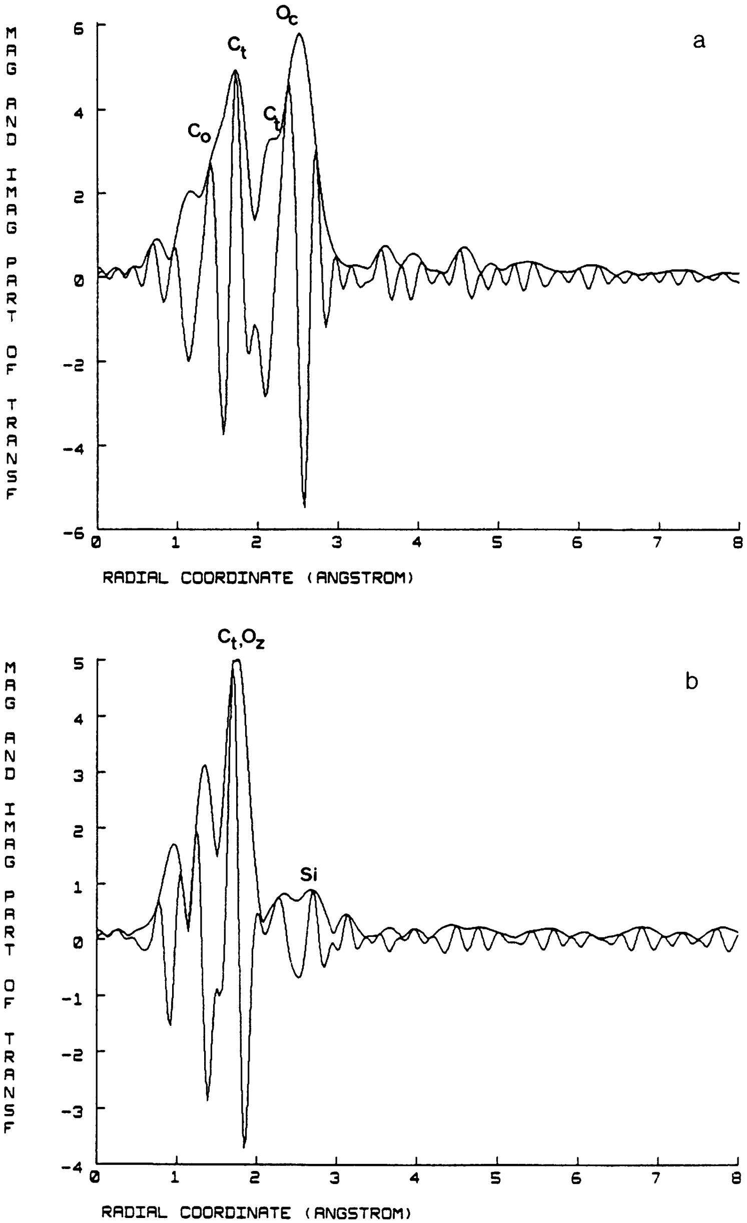

Figure 4. Iron EXAFS spectra of $COTFe(CO)_3$ in acid support HY at a) room temperature and b) 473 K. Labels indicate specific backscatterers as in Figure 3. Ct = Fe-COT.

In partially acidic H2Y/COT, coexistence of $COTFe(CO)_3$ and homotropylium ions is observed (Figure 5a).

It appears that a chemical reaction of the zeolite support with the occluded complex occurs only in the presence of acid groups, resembling the reaction path found in homogeneous medium with non-coordinating acids. Upon heating these samples, TPD-MS experiments do not show any significant fragments related to a loss of the C_8H_9 ligand or the desorption of any other iron-containing fragments. Therefore, these species have to be trapped in the zeolite cage system. The EXAFS analysis of the heated sample shows an organic fragment at R = 2.07 Å in addition to oxygen coordination at R = 2.16 Å (Figure 4b). This product can be described as a $[FeC_8H_9]^+$ fragment which is coordinated to two zeolite oxygens in the large faujasite supercage:

$$[C_8H_9Fe(CO)_3]^+ + (OZ)_2^- \xrightarrow{\Delta T} C_8H_9Fe(OZ)_2 + 3\,CO\,(g)$$

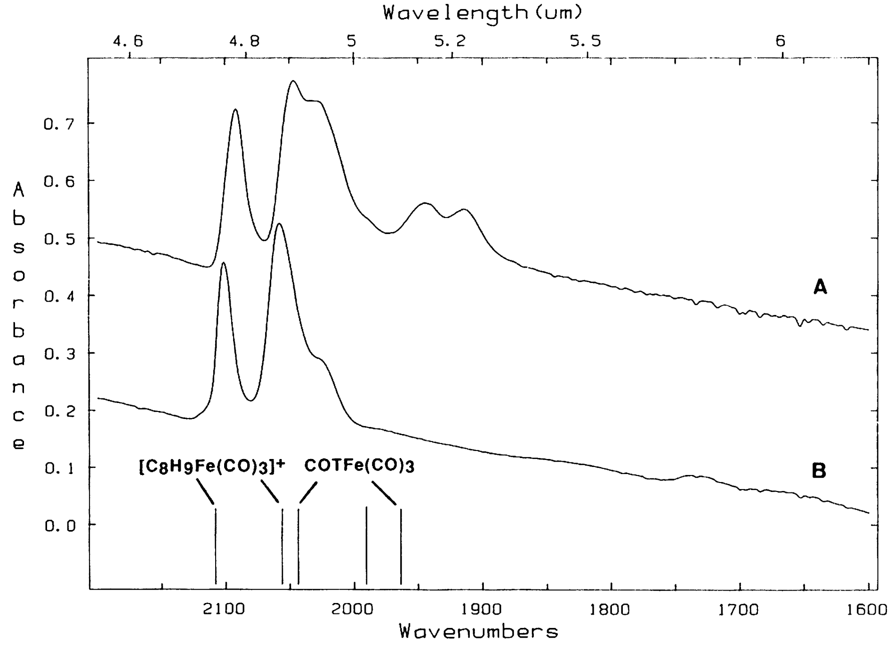

Figure 5. FTIR spectra of $COTFe(CO)_3$ in a) H2Y and b) H6Y, at room temperature. Markers indicate the wavenumbers of unsupported complex $COTFe(CO)_3$ (KBr) and the homotropylium iron tricarbonyl $[C_8H_9Fe(CO)_3]^+$ (in CS_2/CCl_4).

Upon cleavage of the carbonyl ligands, the zeolite oxygens of the supercage SIII four-ring positions fill the coordination sphere of the remaining organometallic iron fragment.

Intrazeolite Chemistry of $CpFe(CO)_2CH_3$

As with the other iron complexes, the reaction of the intrazeolite hydroxyls with $CpFe(CO)_2CH_3$ results in the formation of cationic iron-species, which under thermal treatment decompose to anchored fragments. The IR spectrum of the NaY/MeFp sample shows the presence of $CpFe(CO)_2CH_3$ which interacts with the zeolite sodium cations (Figure 1c). The complex reacts in both moderately and highly acidic zeolites to yield the dicarbonyl cation $CpFe(CO)_2^+$ as well as the tricarbonyl cation $CpFe(CO)_3^+$ as protonation products (Figure 6a,b). The latter is relatively more stable at elevated temperatures. Treatment of $CpFe(CO)_2CH_3$ in solution with acids having a $pK_a < 1$, e.g. CF_3COOH [36], resulted in the

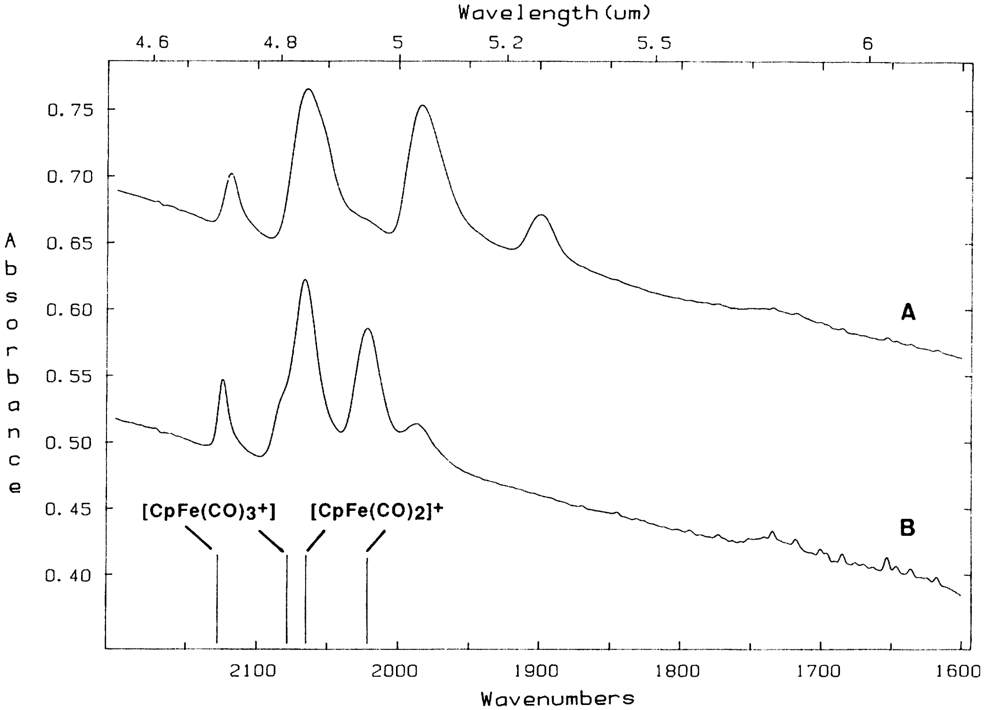

Figure 6. FTIR spectra of $CpFe(CO)_2CH_3$ in a) H2Y and b) in H6Y, at room temperature. Markers indicate the wavenumbers of the cationic complexes $[CpFe(CO)_2]^+$ (in CH_2Cl_2) and $[CpFe(CO)_3]^+$ (in H_2SO_4 film).

exclusive formation of the dicarbonyl cation. The acid zeolites promote a comparable reaction, however, in addition the tricarbonyl cation is formed. This reaction must involve intermolecular CO transfer. Carbonyl transfer has been observed in other systems such as the unsaturated complex $C_4H_7Fe(CO)_3^+$ which spontaneously forms $C_4H_7Fe(CO)_4^+$ [37]. In the zeolite, the formation of tricarbonyl cations must involve partial fragmentation of the dicarbonyl. It is suggested that this fragment is $CpFe^+(OZ)_n$, similar to intrazeolite products of Fp2 (see above). The absence of CH_4 in subsequent TPD-MS experiments indicates that the methyl ligands have already been split off by the zeolite hydroxyls during the loading period of $CpFe(CO)_2CH_3$. These results can be summarized in the following tentative reaction pathway at room temperature:

$$CpFe(CO)_2CH_3 + ZOH \rightarrow [CpFe(CO)_2]^+OZ^- + CH_4 \quad \text{(in slurry)}$$
$$3\,[CpFe(CO)_2]^+ + (OZ)_n^- \rightarrow 2\,[CpFe(CO)_3]^+ + CpFe^+(OZ)_n^-$$

TPD-MS data at elevated temperatures suggest that the loss of carbonyl ligands from both the di- and tricarbonyl cations results in the formation of additional intrazeolite fragment $CpFe^+$:

$$[CpFe(CO)_n]^+ + (OZ)_m^- \xrightarrow{>473\ K} CpFe(OZ)_m + n\,CO\,(g) \qquad n,m = 2,3$$

CONCLUSION

The anchoring strategy demonstrated above is based upon the different reactivities of ligands at a transition metal center towards the bridged hydroxyl groups present in acid large-pore zeolites. It could be shown that under certain conditions the metal attaches to the zeolite oxygen rings while only the most stable ligands are retained at the metal. This technique allows us to obtain control of the *siting* of the immobilized metal fragment. Since the large neutral complexes cannot enter the smaller sodalite and double six-ring cages present in zeolite Y, they are confined to positions in the large supercage. In contrast, the traditional stepwise assembly of intrazeolite complexes from metal ions and small ligands such as CO relies upon preceding aqueous ion exchange and dehydration under drastic conditions. Thus, a large fraction of the metal is forced to migrate into the smaller cavities which are less desirable positions in the context of catalytic applications and which make characterization of the resulting mixture of intrazeolite products very difficult. The alternative procedure developed in the present work results in migration-stabilized fragments chemically anchored into accessible zeolite pores. Our studies are presently being extended to other transition metal/ligand combinations which potentially retain reactive coordination sites after being attached to the zeolite, and to bimetallic complexes with different ligand reactivities.

Acknowledgements. Acknowledgement is made to the Donors of the Petroleum Research Fund, administered by the American Chemical Society, and to the Sandia University Research Program (DOE), for partial support of this research. The operational funds for NSLS beamline X-11A are supported by DOE grant DE-AS0580ER10742.

References

1. Ballivet-Tkatchenko, D.; Coudrurier, G.; Mozzanega, H.; Tkatchenko, I.; Kinnemann, A. *J. Mol. Cat.* **1979**, *6*, 293.
2. Suib, S. L.; Kostapapas, A.; McMahon, K. C.; Baxter, J. C.; Winiecki, A. M. *Inorg. Chem.* **1985**, *24*, 858.
3. Bein, T.; McLain, S. J.; Corbin, D. R.; Farlee, R. F.; Moller, K.; Stucky, G. D.; Woolery, G.; Sayers, D. *J. Am. Chem. Soc.* **1988**, *110*, 1801.
4. Herron, N.; Stucky, G. D.; Tolman, C. A. *Inorg. Chim. Acta* **1985**, *100*, 135.
5. Bein, T.; Schmiester, G.; Jacobs, P. A. *J. Phys. Chem.* **1986**, *90*, 4851.
6. Yang, Y. S.; Howe, R. F. In *New Developments in Zeolite Science and Technology*; Murakami, Y.; Iijima, A.; Ward, J. W., Eds.; Kodansha: Tokyo, 1986; p. 883.
7. Verdonck, J. J.; Schoonheydt, R. A.; Jacobs, P. A. *J. Phys. Chem.* **1983**, *87*, 683.
8. Gelin, P.; Naccache, C.; Ben Taarit, Y.; Diab, Y. *Nouv. J. Chim.* **1984**, *8*, 675.
9. Bergeret, G.; Gallezot, P.; Gelin, P.; Ben Taarit, Y.; Lefebvre, F.; Naccache, C.; Shannon, R. D. *J. Catal.* **1987**, *104*, 279.
10. Davis, M. E.; Schnitzer, J.; Rossin, J. A.; Taylor, D.; Hanson, B. E. *J. Mol. Cat.* **1987**, *39*, 243.

11. Shannon, R. D.; Vedrine, J. C.; Naccache. C.; Lefebvre, F. *J. Catal.* **1984**, *88*, 431.
12. Rode, E. J.; Davis, M. E.; Hanson, B. E. *J. Catal.* **1985**, *96*, 574.
13. Herron, N. *Inorg. Chem.* **1986**, *25*, 4714.
14. Diegruber, H.; Plath, P. J.; Schulz-Ekloff, G. *J. Mol. Cat.* **1984**, *24*, 115.
15. Herron, N.; Stucky, G. D.; Tolman, C. A. *J. Chem. Soc., Chem. Commun.* **1986**, 1521.
16. Yermakov, Yu. I. *Catal. Rev.-Sci. Eng.* **1976**, *13*, 77.
17. Foley, H. C.; DeCanio, S. J.; Tau, K. D.; Chao, K. J.; Onuferko, J. H.; Dybowski, C.; Gates, B. C. *J. Am. Chem. Soc.* **1983**, *105*, 3074.
18. Ward, M. D.; Schwartz, J. *J. Mol. Cat.* **1981**, *11*, 397.
19. Huang, T. N.; Schwartz, J.; Kitajima, N. *J. Mol. Cat.* **1984**, *22*, 389.
20. Huang, T. N.; Schwartz, J. *J. Am. Chem. Soc.* **1982**, 104, 5244.
21. Corbin, D. E.; Seidel, W. C.; Abrams, L.; Herron, N.; Stucky, G. D.; Tolman, C. A. *Inorg. Chem.* **1985**, *24*, 1800.
22. Taylor, D. F.; Hanson, B. E.; Davis, M. E. *Inorg. Chim. Acta* **1987**, *128*, 55.
23. Moller, K.; Borvornwattananont, A.; Bein, T. *J. Phys. Chem.* **1989**, *93*, 4562.
24. Borvornwattananont, A.; Moller, K.; Bein, T. *J. Phys. Chem.* **1989**, *93*, 4205.
25. Lee, P. A.; Citrin, P. H.; Eisenberger, P.; Kincaid, B. M. *Rev. Mod. Phys.* **1981**, *53*, 769.
26. Johnson, E. C.; Meyer, T. J.; Winterton, N. *J. Chem. Soc., Chem. Commun.* **1970**, 934.
27. Johnson, E. C.; Meyer, T. J.; Winterton, N. *Inorg. Chem.* **1971**, *10*, 1673.
28. Dombeck, B. D.; Angelici, R. J. *Inorg. Chim. Acta* **1973**, *7*, 345.
29. Boyle, P. F.; Nicholas, K. M. *J. Organomet. Chem.* **1976**, *114*, 307.
30. Catheline, D.; Astruc, D. *J. Organomet. Chem.* **1984**, *266*, C11.
31. Davison, A.; Green, M. L. H.; Wilkinson, G. *J. Chem. Soc.* **1961**, 3172.
32. Beaumont, R.; Barthomeuf, D.; Trambouze, Y. *Adv. Chem. Ser.* **1971**, *102*, 327.
33. Legzdins, P.; Martin, D. T.; Nurse, C. R.; Wassink, B. *Organometallics* **1983**, *2*, 1238.
34. Woolery, G.; Kuehl, G.; Chester, A.; Bein, T.; Stucky, G. D.; Sayers, D. E. *J. Physique.* **1986**, *47*, C8-281.
35. Darensbourg, M. Y.; Barras, H. L. C. *Inorg. Chem.* **1979**, *18*, 3286.
36. De Luca, N.; Wojcicki, A. *J. Organomet. Chem.* **1980**, *193*, 359.
37. Gibson, D. H.; Vonnahme, R. L. *J. Am. Chem. Soc.* **1972**, *94*, 5090.